

***Final Draft***  
of the original manuscript:

Chen, F.; Storch, H.v.; Zeng, L.; Du, Y.:  
**Polar Low genesis over the North Pacific under different  
global warming scenarios**  
In: *Climate Dynamics* (2014) Springer

DOI: 10.1007/s00382-014-2117-5

# Polar Low genesis over North Pacific under different scenarios of Global Warming

Fei Chen<sup>1,2</sup>, Hans von Storch<sup>1</sup>, Yan Du<sup>3</sup>, Lun Wu<sup>1</sup>

1. Institution of Remote Sensing and Geographical Information System, School of Earth and Space Sciences, Peking University, Beijing, China

2. Helmholtz-Zentrum Geesthacht, Max-Planck-Str. 1, Geesthacht, Germany

3. South China Sea Institute of Oceanology, Chinese Academy of Science, Guangzhou, China

## Abstract:

Following an earlier climatology study of North Pacific Polar Lows by employing a dynamical downscaling of NCEP 1 reanalysis using the regional climate model COSMO-CLM, the characteristics of Polar Low genesis under different global warming scenarios are investigated. Three SRES scenarios run with a global climate model (ECHAM5) are examined if we may expect systematic changes in the formation of Polar Lows over the next century. The results show that with more greenhouse gas emission, global warming and the air temperature rising, the frequency of Polar Lows is decreasing. With sea ice melting, the distribution of Polar Low genesis shows a northward shift. In scenarios with stronger warming, the trend towards less Polar Lows gets larger.

## 1. Introduction

The North Pacific is an area where frequently sub-synoptic Polar Lows form in the cold season (Rasmussen and Turner 2003) in association with cold air outbreak. Because of the strong wind speeds and heavy rainfall, Polar Lows represent a significant weather climate risk which threatens maritime human activities.

Multi-decadal reanalysis, such as those provided by NCEP or ECMWF, as well as climate change scenarios, as those in the CMIP ensembles, do not allow the determination of changing statistics of Polar Lows, because the spatial scale of these disturbances is insufficiently resolved in such data sets. Therefore dynamical downscaling efforts have been carried out, which employ regional climate models, to determine the multi-decadal climatology of Polar Lows (Chen and von Storch 2013). To do so, a regional climate model was conditioned by large-scale information of NCEP re-analyses. It turned out that in this way the formation and life cycles of Polar Lows during the past decades could be reconstructed homogeneously without exploiting sub-synoptic information in initial fields (Chen et al. 2012).

This approach is now used to determine, how the frequency of emergence of Polar Lows is changing in a series of scenarios describing the response of the climate system to three SRES

34 emission scenarios from the Intergovernmental Panel on Climate Change (IPCC) developed for  
35 the Assessment Reports 3 and 4.

36 In section 2 we briefly describe the data and methodology of the simulation and  
37 tracking algorithm. Section 3 is divided into three parts in order to determine (decreasing) trends  
38 in discuss the Polar Low genesis, variations of the trend associated with different greenhouse gas  
39 emission scenarios and the spatial (northward) shift of Polar Low genesis. The paper is concluded  
40 with a discussion and summary in the final section 4.

## 41 **2. Methodology and data**

### 42 **Downscaling and tracking**

43 The basic concept is to dynamically downscale scenario simulations with a global model for  
44 the region of the North Pacific. For doing so, the COSMO-CLM (Steppeler et al. 2003) was used as  
45 regional climate model. The COSMO-CLM (COSMO model in CLimate Mode) is the climate version  
46 of the operational weather prediction model of the Deutscher Wetterdienst and the COnsortium  
47 for SMalL scale MOdelling (COSMO), adapted to climate simulation purposes by the  
48 CLM-Community (<http://www.clm-community.eu>).

49 The states in the global climate change simulations are fed into the regional model at the  
50 lateral boundaries and lower boundary. Similar as a previous climatological study (Chen and von  
51 Storch, 2013), which downscaled NCEP 1 reanalyses, the spectral nudging is employed also.

52 The CCLM model is capable to generate Polar Lows, without providing seeds in initial states  
53 (Chen et al., 2012). These Polar Lows are detected and tracked by using a modified algorithm  
54 developed by Zahn and von Storch (2008). For detailed information of the model, the  
55 downscaling technology and the tracking algorithm the reader is referred to the previous study  
56 (Chen et al. 2012; Chen and von Storch 2013).

### 57 **Scenario Information**

58 The scenarios we applied here are designed by the IPCC in 2000 (Nakicenovic et al.  
59 2000) known as the Special Report on Emissions Scenarios (SRES). The SRES scenarios consider a  
60 wide range of factors, such as population, industrialization, urbanization, social and economic  
61 developments to estimate the greenhouse gas emission. These emission scenarios are fed into  
62 global climate models for studying the effect of increasing greenhouses gas concentrations on the  
63 possible future state of the climate system,, such as: investigating the changes of storm and  
64 cyclone activity under different SRES scenarios (Pinto et al. 2007) and increased precipitation  
65 intensity (Meehl, Arblaster, and Tebaldi 2005). Various characteristics which reflected the  
66 response of the climate system to different scenarios are also investigated and described by the  
67 scientists. Such as: the air temperature, precipitation, sea level raise, sea ice melting, ocean  
68 current circulation change, extremely weather phenomenon, aerosols and carbon dioxide cycle  
69 variability in climate (Stocker and Schmittner 1997; Boer, Flato, and Ramsden 2000; Cox et al.  
70 2000; Friedlingstein et al. 2001; Yonetani and Gordon 2001).

71           **Forcing data: ECHAM5**

72           The global climate model used was the coupled GCM ECHAM5/MPI-OM1 (Roeckner et  
73 al. 2003) which refers the European Centre Hamburg Version 5/Max-Planck-Institute – Ocean  
74 Model Version 1. Detailed information is available in the documentations (Roeckner et al. 2003;  
75 Marsland et al. 2003; Jungclaus et al. 2005). The different scenario runs were initiated in the year  
76 “1948” and run until “2000” with observed forcing, and then the scenario-runs were extended  
77 until 2100. Three such simulations with A1B, labeled A1B\_1, A1B\_2 and A1B\_3, were run with  
78 ECHAM5/MPI-OM and then dynamically downscaled with CCLM. Similarly one scenario exposed  
79 to B1 and A2 emission scenarios were processed. The output of the global runs was archived by  
80 CMIP5.

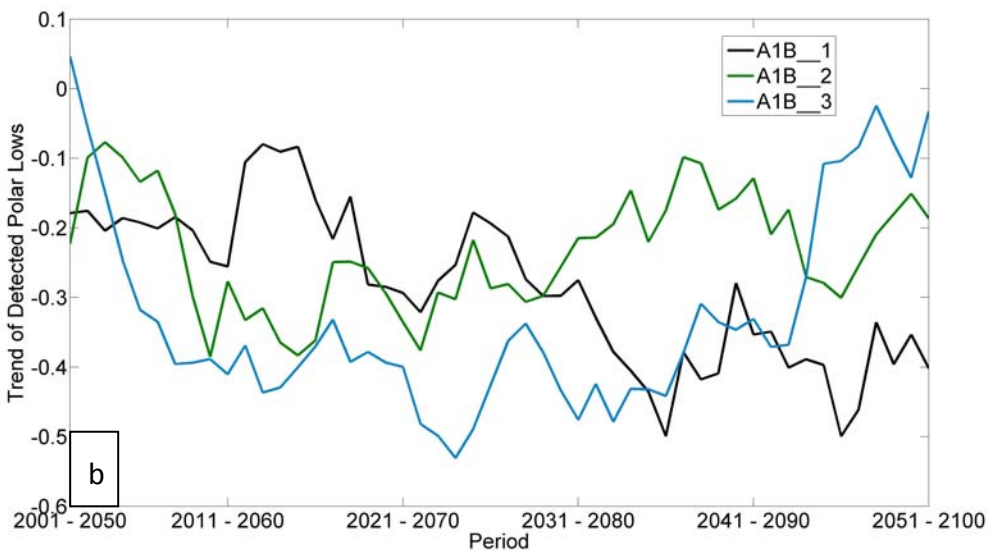
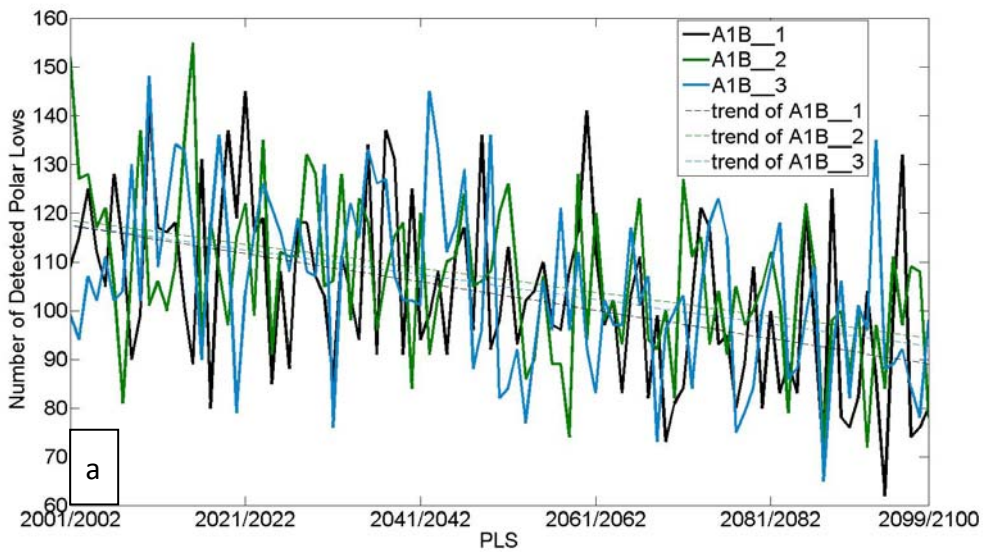
## 81           **3. Simulation and tracking results**

82           Polar Lows form in winter, therefore the “Polar Low season” (PLS) is defined as  
83 extending from October through next April. The Polar Low season is addressed by the first and  
84 second year, for example the PLS 2001/2002 begins in October 2001 and ends in April 2002. For  
85 each PLS we present in the following the number of detected North Pacific Polar Lows.

### 86           **3.1 Analysis of A1B scenarios**

87           For demonstrating the effect of the increasing CO<sub>2</sub> concentrations to the frequency of  
88 North Pacific Polar Lows formation, we take A1B as example. Figure 1a presents the time series of  
89 detected Polar Lows per PLS and the corresponding trend over the next century under the three  
90 realizations of A1B. They all share a negative trend and there is no obvious significant difference  
91 between the three realizations. Namely the trend for A1B\_1 is -0.29 cases/PLS; for A1B\_2 is -0.24  
92 cases/PLS and for A1B\_3 is -0.25 cases/PLS, with a corresponding standard deviation of 18.19,  
93 16.12 and 17.49.

94           Figure 1b shows running 50 years trends of the three 2000-2099 series with A1B scenarios.  
95 The downturn of the number of cases varies somewhat in time, but is steady. When examining 30  
96 and 40 years trends (not shown), a similar situation emerges, even though the variability of the  
97 series becomes much larger.

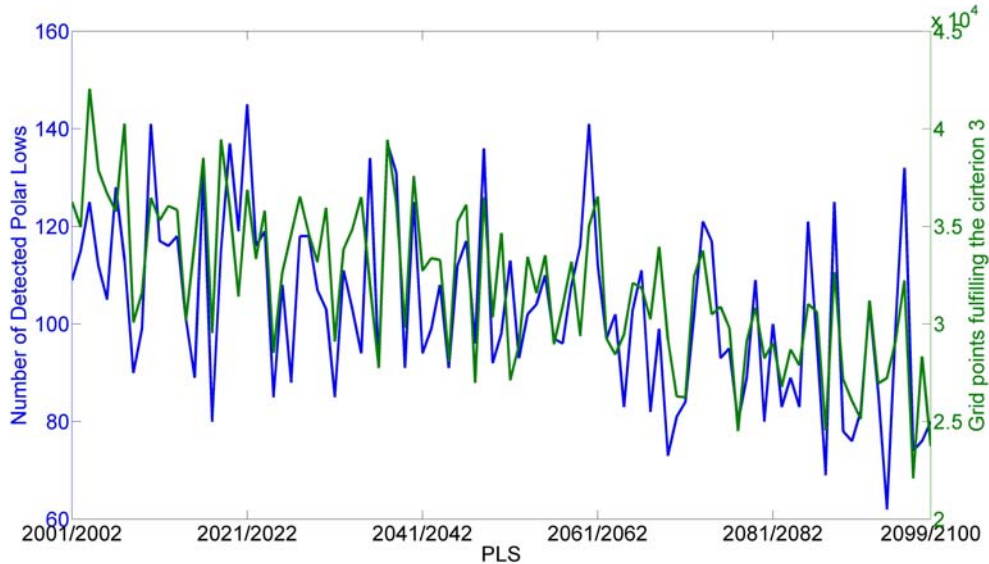


101 *Figure 1 a) Number of Detected Polar Lows per PLS simulation) and three realizations of A1B scenario,*  
 102 *2001/2002 – 2009/2100. The straight lines represent the trends for the three A1B developments.*

103 *b) Running 50-years trends of the three combined series of detected Polar Lows per PLS in A1B; the trends are*  
 104 *labeled with the first year of the moving 50 year window.*

105 As Zahn and von Storch (2010) pointed out for the Polar Low frequency over the North  
 106 Atlantic in the next century, that both the SST of the Atlantic and the tropospheric air  
 107 temperature are getting warmer. However, the rise of tropospheric air temperature is higher than  
 108 the rise of the SST, so that the troposphere-sea temperature difference is getting smaller, so that  
 109 the vertical stability is getting higher. The increased stability is less favorable for Polar Low genesis.  
 110 To demonstrate that this mechanism is also operating in the North Pacific, we determined the

111 seasonal temperature difference between the 500 hPa level and the seas surface for A1B\_1. Only  
 112 points with open water, i.e., no sea ice, were considered. We count the number of points for each  
 113 PLS, where the mean air-sea temperature is equal or larger than 39 K. When this is the case we  
 114 refer to “critical temperature difference”



115

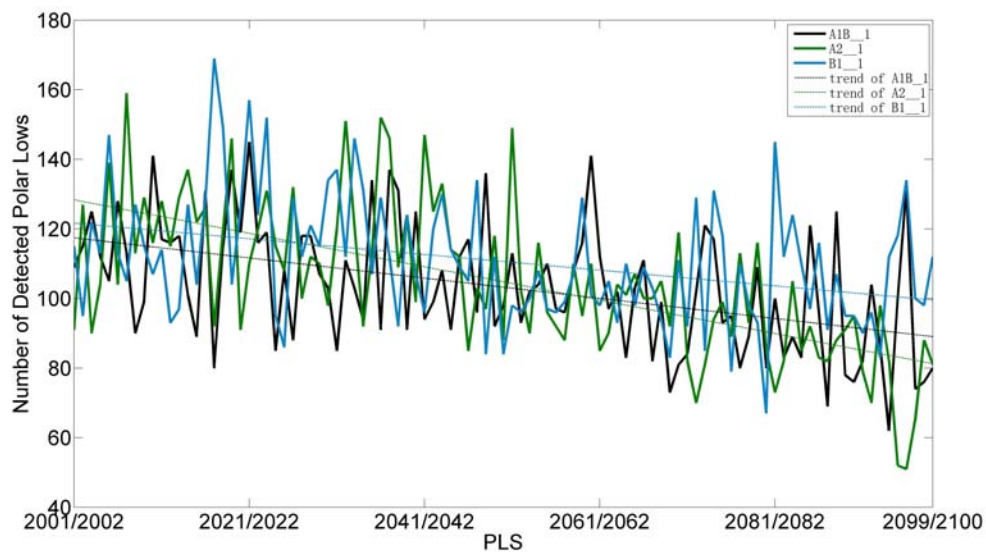
116 *Figure 2: Development of PLS-number of Polar Lows, derived from detecting and tracking (in blue) and*  
 117 *percentage of open-sea grid points, with a vertical temperature gradient beyond the critical 39K (red).*

118 Since the number of points without sea ice is increasing, we show in Figure 2 the percentage  
 119 of such points with a critical vertical temperature difference compared to the overall number of  
 120 eligible (ice free sea) points. For A1B\_1 this percentage decreases by 29% to the end of 21<sup>th</sup>  
 121 century compared to the beginning (the corresponding trend is -93.53 grid points per PLS), for  
 122 A1B\_2 and A1B3 it is 24% with -71.31 grid points/PLS and 22% with -70.14 grid points/PLS. Thus,  
 123 favorable conditions for Polar Low genesis decreased nearly one third since the beginning of this  
 124 century for all three realizations of A1B simulations. The comparison with the directly detected  
 125 and tracked Polar Lows, also shown in Figure 2, confirms that the proxy “Vertical temperature  
 126 difference” describes adequately the decreasing trend in Polar Low activity for the 21<sup>th</sup> century:  
 127 The correlation between the two curves, after subtraction of their trends, amounts to 74.4%. For  
 128 A1B\_2 it is 72.8%, for A1B\_3 is 79.1% (not shown)

129

## 130 **2 Other Greenhouse Gas emission scenarios**

131 As shown in Figure 1a, there is no obvious significant difference between different  
 132 realizations of single story line. Therefore and for reasons of computational cost and time we only  
 133 take the first realization for the different scenarios such as A2\_1 and B1\_1. In the following we  
 134 refer only to A1B, A2 and B1.



135

136 *Figure 3: Number of Detected Polar Lows and corresponding trends from 2001/2002 to 2099/2100 of A1B,*  
 137 *A2 and B1.*

138 Figure 3 presents the different tracking results for the three different emission  
 139 scenarios. In all, the number of Polar Lows is decreasing: The trend of A1B is -0.29 case/PLS; for  
 140 the scenario of A2, which has a much higher greenhouse gas emission, the trend is -0.49  
 141 cases/PLS. For B1\_1 the trend is much smaller, with only -0.2 case/PLS. We find that with a higher  
 142 greenhouse gas emission, the frequency of Polar Low occurrence has a correspondingly stronger  
 143 decreasing trend. This is also supported by a general decrease of grid points where the mean  
 144 vertical temperature is beyond the critical 39K (not shown).

145 We have inferred that there will be a lower trend of Polar Low occurrence frequency  
 146 over the North Pacific in the next century under a global warming situation with a higher  
 147 greenhouse gas emission. The higher air temperature raise, the lower air-sea temperature  
 148 differences drop. Consistently, the frequency of favorable conditions for Polar Low genesis is  
 149 declines (Figure ).

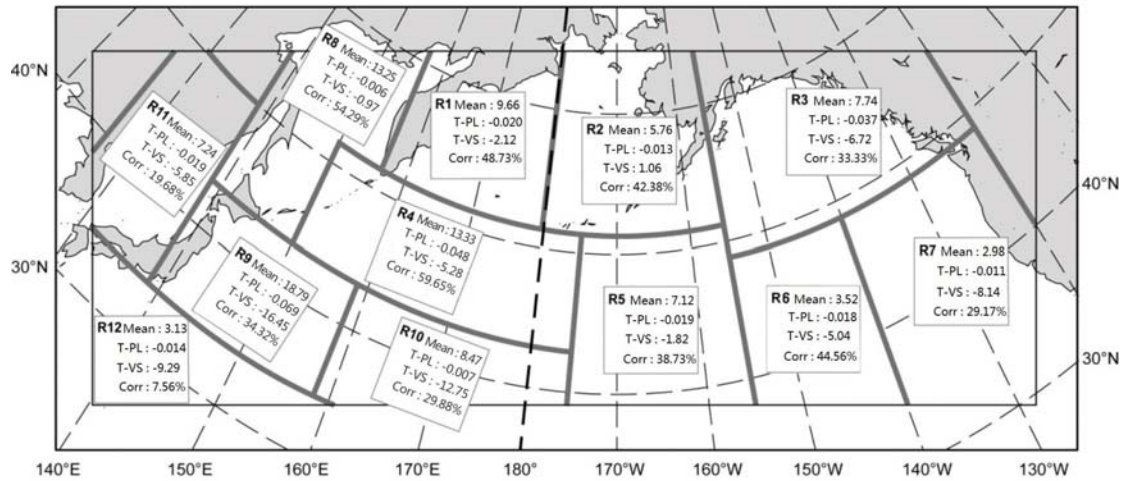
### 150 **3.3 Northward shift of Polar Low genesis associated** 151 **with ice edge melting**

152 For the next step, we are interested on the spatial distribution of Polar Low genesis and  
 153 its variability under future global warming scenario. Here we take A1B as an example. For doing  
 154 so, the North Pacific was divided into 12 sub-regions to compare the Polar Low information in  
 155 different areas. The same sub-regions have been used by Chen and von Storch (2013) to describe  
 156 the present spatial statistics of the formation of Polar Lows. The density of Polar Low genesis, the  
 157 trends in number and in changes of the vertical stability, as well as the correlation of the two

158 measures of Polar Low genesis in the 12 sub-regions in the next century are presented in Figure  
159 4.

160 The region of highest Polar Low density is located to the east ocean of Japan Island (R9), the  
161 smallest values in R21 in the far southwest, and R6 and R7 in the southeast - in consistence with  
162 the climatology of last six decades. The most trends are in all 12 sub-regions negative, both in  
163 terms of detected and tracked polar lows, and in terms of the proxy "spatial percentage of critical  
164 vertical temperature difference" (in R2 the trend is small, albeit positive). The two measures are  
165 all positively correlated (after taking out the trends), with a maximum of 60% in R4 west of the  
166 dateline and a minimum 8% in R12 in the far southwest of the area.

167 The strongest decline trend of Polar Lows genesis per open-sea grid point is found in R9 east  
168 of Japan with  $-6.9 \times 10^{-2}$  cases per grid point per PLS. In R4 the trend is with  $-4.8 \times 10^{-2}$  cases per grid  
169 point per PLS. For the sub-regions R1, R5, R6 and R11, the trends in detected and tracked Polar  
170 lows is about  $2 \times 10^{-2}$  cases per open-sea grid point per PLS; in the other sub-regions the trends  
171 are smaller.



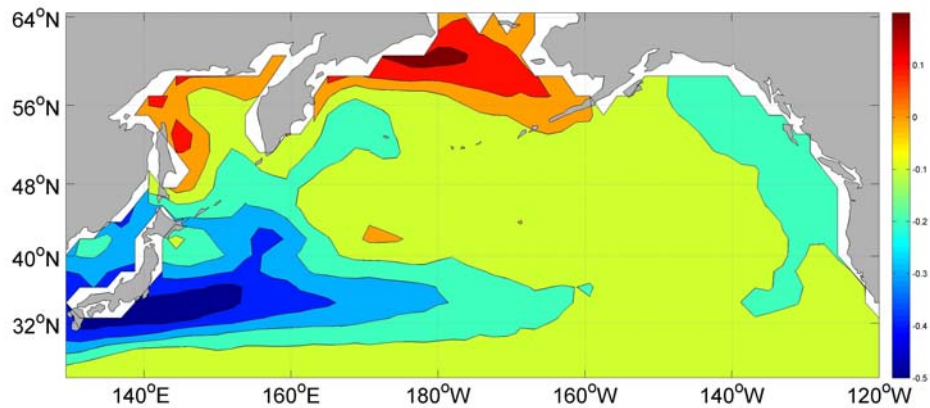
172  
173 *Figure 4: Sub-regions, for which the numbers (Mean) of and trends in detected (T-PL), or estimated (T-VS)*  
174 *Polar Lows formation were aggregated (R1-R12). Also given are the correlations (corr) between the detected*  
175 *and estimated Polar occurrence (after subtracting trends). The estimated number is the percentage of open-sea*  
176 *grid points in each sub-region, where the critical temperature difference between the sea surface and 500 hPa*  
177 *of 39K or more is met.*

178 The correlated measure of percentage of open-sea points with a vertical difference of 39K  
179 and beyond shows a similar pattern, with mostly negative trends (labeled T-VS in Figure 4), but  
180 one, albeit very small positive trend in R2. In general, the trends in the Northwest, in R1, R2 and  
181 R8, exhibit small trends, while in the other sub-regions the trends are solidly negative, with  
182 largest values in R9 and R10.

183 The correlation of the 12 trends, derived from the tracking data, and derived from the  
184 change in vertical temperature differences, amounts to 43%.

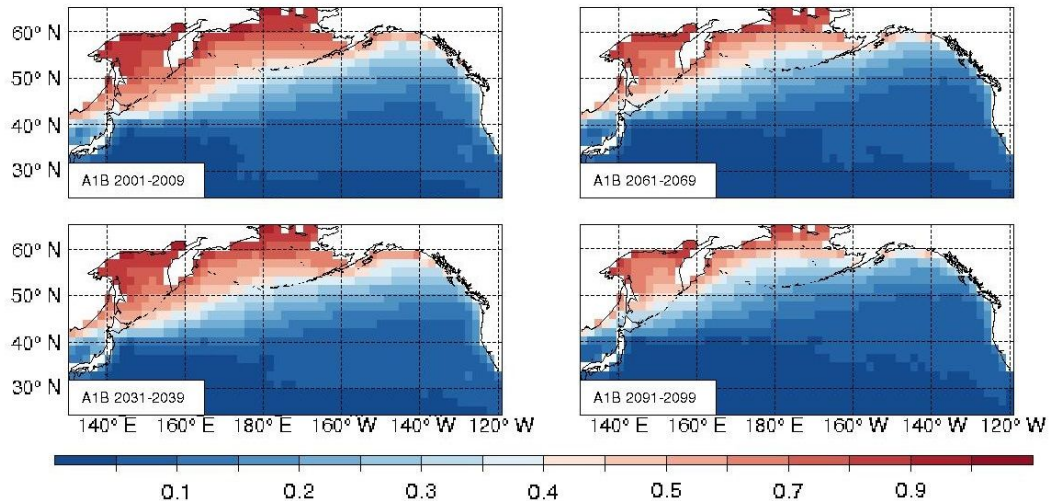


185 Another similar measure is the trend in the number of times, on the basis of four-times daily  
186 grid point data, per PLS with a critical temperature difference of 39 K and more (Figure 5).  
187 (Before, we had examined the percentage of points with a critical difference in the seasonal  
188 mean; here we determine the change of the percentage in time per PLS.) The frequency of  
189 relatively more stable conditions, when the 39 K difference is not met, increases almost  
190 everywhere in the North Pacific Basin, with maximum values of -0.5 grid points/PLS east of Japan  
191 – but also larger regions in the North. Consistently the largest differences in the emergence of  
192 Polar Lows are in the Northwest Pacific, and the weakest are where red colors dominate in Figure  
193 5. The tendency towards more stable conditions in most of the region reflects the faster warming  
194 of the troposphere, and the slower warming at the sea surface. The red regions point to the  
195 retreat of sea ice in the course of the overall warming (Figure 6).



196

197 *Figure 5: Trends of the frequency of number of times (of 4-times daily values) within a PLS, when the*  
198 *vertical temperature difference (SST - 500 hPa temperature) is 39K or more. Red colors point to more frequent*  
199 *more stable conditions, while blue indicate less frequent such conditions. Units: grid points/PLS.*



200

201 *Figure 6: Mean proportion of ice covered time over the North Pacific Ocean during the PLS for different 10*  
 202 *year means: 2001-2009, 2031-2039, 2061-2069 and 2091-2099 are calculated from the ECHAM5/MPI-OM1 of*  
 203 *A1B\_1.*

204 Figure 6 demonstrates this gradual decrease of the sea ice in the northern parts of the  
 205 region. During the first decade, 2001-1009, sea ice is present in most part of the sea of Okhotsk  
 206 and Bering Sea during 70% of a PLS. In the Gulf of Alaska also nearly 50% of the time the sea is  
 207 frozen along the north coast. But for the last 70 PLSs during 2031 – 2099, the proportion of sea  
 208 ice during winter is gradually decreasing. In the Okhotsk and Bering Sea and in the Gulf of Alaska,  
 209 the time of frozen conditions is dropped by 55% at the end of next century in this scenario.

210 When the sea ice edge is retreating, the cold air flow from the north meets the relative  
 211 warm SST earlier on its southward movement. Thus, in these regions, such as R1 and R8, the  
 212 reduction of numbers of Polar Lows is smallest. At the same time, the cold continental air has to  
 213 travel a longer distance across the warmer SST before reaching the more southern regions, so  
 214 that there the tendency for forming Polar Lows in R4 and R9 is further reduced.

215 For comparing the strengths of the trends between the sub-regions, we calculated area  
 216 weighted mean of their trends by divided the overall trends by the number sea grid points for  
 217 each sub-region. The overall trend of detected Polar Lows is negative with  $-0.29$  cases/PLS, which  
 218 amounts to  $-2.7 \times 10^{-5}$  cases per PLS per grid point. The trends in different sub-regions are not  
 219 uniform. R9 exhibits the strongest decrease trend of  $-8.3 \times 10^{-5}$  cases per PLS per grid point. For R1,  
 220 R4 and R11 somewhat smaller decreasing trends prevail:  $-2.0 \times 10^{-5}$ ,  $-4.8 \times 10^{-5}$ , and  $-6.9 \times 10^{-5}$ . The  
 221 R8-trend is the weakest  $-0.9 \times 10^{-5}$  cases per PLS per grid point. This pattern describes a relative  
 222 northward shift of Polar Low distribution in the coming 100n years of the scenario A1B.

223 In the A2 and B1 scenarios the changes of sea ice melting and a northward shift of Polar Low  
 224 formation are similar to A1B (not shown). With more or less CO<sub>2</sub> emission and global warming,  
 225 the Polar Low formation appears to migrate more, or less, northward.

226

## 4. Conclusion

227 We applied global climate model products under different scenarios of societal development  
228 in the future, which go along with different greenhouse gas emissions and global warming  
229 developments. Corresponding spatial distribution of genesis and the trend of Polar Low  
230 occurrence frequency are calculated by a model-based methodology which we had developed for  
231 a hind cast of the last 62 years conditions 1948 to 2010 (Chen and von Storch, 2013).

232 A general idea is that the frequency of Polar Low occurrence has a close relationship with  
233 the global warming. With a stronger increase of the CO<sub>2</sub> emission the frequency is decreasing  
234 much more rapidly than with smaller increases. The spatial distribution shows a northward shift  
235 through next century under the different scenarios. The explanation for this change is mainly  
236 related to the raised atmosphere temperatures, less fast warming of the sea surface and a  
237 gradual retreat of the northern ice cover. The decrease of air-sea temperature difference leads to  
238 reduced vertical instability. With less frequent favorable condition, the frequency of Polar Low  
239 occurrence is decreasing; with melting sea ice and northward ice edge, the Polar Lows forms  
240 more northward compared than in earlier times.

241 We have to point out that our regional simulation is a scenario, i.e., a possible and  
242 consistent description of future conditions related only to greenhouse gas and aerosol emissions,  
243 but not a prediction of what may be considered the most probable development expected to  
244 happen in the coming 90 years.

245

## Acknowledgement

246 The work was done with the support of the Chinese Scholarship Council CSC, and it is a  
247 contribution to the Helmholtz Climate Initiative REKLIM (Regional Climate Change), a joint  
248 research project of the Helmholtz Association of German Research Centers. The authors thank  
249 Beate Gardeike for preparing most of the diagrams. The technical and scientific support, the  
250 various comments and suggestions by Dr. Beate Geyer and Dr. Matthias Zahn have greatly  
251 improved this manuscript.

252

## Reference

253 Boer, G.J., G. Flato, and D. Ramsden, 2000: A Transient Climate Change Simulation with  
254 Greenhouse Gas and Aerosol Forcing: Projected Climate to the Twenty-first Century. *Climate*  
255 *Dynamics* 16: 427–450.

256 Chen, Fei, Beate Geyer, Matthias Zahn, and Hans von Storch, 2012: Towards a  
257 Multi-Decadal Climatology of North Pacific Polar Lows Employing Dynamical Downscaling. *Terr.*  
258 *Atmos. Ocean. Sci.* 23(3): 291–301.

259           Chen, Fei, and Hans von Storch, 2013: Trends and Variability of North Pacific Polar Lows.  
260           Advances in Meteorology. <http://dx.doi.org/10.1155/2013/170387>

261           Cox, P.M., R.A. Betts, C.D. Jones, S.A. Spall, and I.J. Totterdell, 2000: Acceleration of Global  
262           Warming Due to Carbon-cycle Feedbacks in a 3D Coupled Climate Model. *Nature* 408: 184–187.

263           Friedlingstein, P., L. Bopp, P. Ciais, et al., 2001: Positive Feedback Between Future Climate  
264           Change and the Carbon Cycle. *Geophys. Res. Lett* 28(8): 1543.

265           Jungclaus, J.H., M. Botzet, H. Haak, et al., 2005: Ocean Circulation and Tropical Variability  
266           in the Coupled Model. *ECHAM5/MPI-OM. J. Climate* 19: 3952–3972.

267           Marsland, S.J., H. Haak, J.H. Jungclaus, M. Latif, and F. Röske, 2003: The  
268           Max-Planck-Institute Global Ocean/sea Ice Model with Orthogonal Curvilinear Coordinates.  
269           *Ocean Model* 5: 91–127.

270           Meehl, Gerald A., Julie M. Arblaster, and Claudia Tebaldi, 2005: Understanding           Future  
271           Patterns of Increased Precipitation Intensity in Climate Model Simulations. *Geophys. Res. Lett.* 32:  
272           L18719.

273           Nakicenovic, N., J. Alcamo, G. Davis, et al., 2000: Special Report on Emissions Scenarios: a  
274           Special Report of Working Group III of the Intergovernmental Panel on Climate Change.  
275           <http://www.ipcc.ch/ipccreports/sres/emission/index.php?idp=0>.

276           Pinto, J. G., U. Ulbrich, G. C. Leckebusch, et al., 2007: Changes in Storm Track and Cyclone  
277           Activity in Three SRES Ensemble Experiments with the ECHAM5/MPI-OM1 GCM. *Clim. Dynam.* 29:  
278           195–210.

279           Rasmussen, Erik A., and John Turner, 2003: Polar Lows: Mesoscale Weather Systems in the  
280           Polar Regions. Cambridge University Press.

281           Rockel, Burkhardt, Christopher L. Castro, Roger A. Pielke Sr., Hans von Storch, and Giovanni  
282           Leoncini, 2008:           Dynamical Downscaling: Assessment of Model System Dependent Retained  
283           and Added Variability for Two Different Regional Climate Models. *Journal of Geophys. Res.* 113.

284           Roeckner, E., G. Bauml, L. Bonaventura, et al., 2003: The Atmospheric General Circulation  
285           Model ECHAM5. PART I: Model Description. Hamburg: Max-Planck-Institut für Meteorologie.

286           Roeckner, Erich, Michael Lautenschlager, and Heiko Schneider, 2006: IPCC-AR4  
287           MPI-ECHAM5\_T63L31 MPI-OM\_GR1.5L40 SRESA1B Run No.1: Atmosphere 6 HOUR Values  
288           MPImet/MaD Germany. World Data Center for Climate.  
289           [http://dx.doi.org/10.1594/WDCC/EH5-T63L31\\_OM-GR1.5L40\\_A1B\\_1\\_6H](http://dx.doi.org/10.1594/WDCC/EH5-T63L31_OM-GR1.5L40_A1B_1_6H).

290           2006a IPCC-AR4 MPI-ECHAM5\_T63L31 MPI-OM\_GR1.5L40 SRESA1B Run No.2:  
291           Atmosphere 6 HOUR Values MPImet/MaD Germany. World Data Center for Climate.  
292           [http://dx.doi.org/10.1594/WDCC/EH5-T63L31\\_OM-GR1.5L40\\_A1B\\_2\\_6H](http://dx.doi.org/10.1594/WDCC/EH5-T63L31_OM-GR1.5L40_A1B_2_6H).

293           2006b IPCC-AR4 MPI-ECHAM5\_T63L31 MPI-OM\_GR1.5L40 SRESA1B Run No.3:  
294           Atmosphere 6 HOUR Values MPImet/MaD Germany. World Data Center for Climate.  
295           [http://dx.doi.org/10.1594/WDCC/EH5-T63L31\\_OM-GR1.5L40\\_A1B\\_3\\_6H](http://dx.doi.org/10.1594/WDCC/EH5-T63L31_OM-GR1.5L40_A1B_3_6H).

296           2006d IPCC-AR4 MPI-ECHAM5\_T63L31 MPI-OM\_GR1.5L40 SRESA2 Run No.1:  
297           Atmosphere 6 HOUR Values MPImet/MaD Germany. World Data Center for Climate.

298 [http://dx.doi.org/10.1594/WDCC/EH5-T63L31\\_OM-GR1.5L40\\_A2\\_1\\_6H](http://dx.doi.org/10.1594/WDCC/EH5-T63L31_OM-GR1.5L40_A2_1_6H).  
299 2006e IPCC-AR4 MPI-ECHAM5\_T63L31 MPI-OM\_GR1.5L40 SRESB1 Run No.1:  
300 Atmosphere 6 HOUR Values MPImet/MaD Germany. World Data Center for Climate.  
301 [http://dx.doi.org/10.1594/WDCC/EH5-T63L31\\_OM-GR1.5L40\\_B1\\_1\\_6H](http://dx.doi.org/10.1594/WDCC/EH5-T63L31_OM-GR1.5L40_B1_1_6H).  
302 Steppeler, J, G Doms, U Schättler, et al., 2003: Meso-gamma Scale Forecasts Using the  
303 Nonhydrostatic Model LM. *Meteorology and Atmospheric Physics* 82(1): 75–96.  
304 Stocker, T. F., and A. Schmittner, 1997: Influence of CO2 Emission Rates on the Stability of  
305 the Thermohaline Circulation. *Nature* 388: 862–865.  
306 Yonetani, T., and H.B. Gordon, 2001: Simulated Changes in the Frequency of Extremes  
307 and Regional Features of Seasonal/Annual Temperature and Precipitation When Atmospheric  
308 CO2 Is Doubled. *Journal Of Climate* 14(8): 1765–1779.  
309 Zahn, M., and H. von Storch, 2008: Tracking Polar Lows in CLM. *Meteorologische*  
310 *Zeitschrift* 17(4): 445–453.  
311 Zahn, Matthias, and Hans von Storch, 2010: Decreased Frequency of North Atlantic Polar  
312 Lows Associated with Future Climate Warming. *Nature* 467(7313): 309–312.  
313